Dalton Transactions

Cite this: *Dalton Trans.*, 2012, **41**, 5177

www.rsc.org/dalton

PAPER

Photovoltaic and electrocatalytic properties of novel ball-type phthalocyanines bridged with four dicumarol†

Ümit Salan,*[a] Ahmet Altındal,[b] Ali Rıza Özkaya,[a] Bekir Salih[c] and Özer Bekaroğlu*[d]

Received 30th December 2011, Accepted 17th February 2012
DOI: 10.1039/c2dt12510b

The new ball-type metallo bisphthalocyanines (Co_2Pc_2 and Zn_2Pc_2) were synthesized from the corresponding [4,4′-bis(dicoumaroylphthalonitrile)] which can be obtained from the reaction of 3,3′-methylenebis(4-hydroxy-2*H*-chromen-2-one) and 4-nitrophthalonitrile. The structures of the newly synthesized compounds have been confirmed and characterized by elemental analysis, UV/Vis, IR and ^{1}H NMR spectroscopies and MALDI-TOF mass spectrometry. Solar cells of the configuration ITO/Co_2Pc_2/C60/Al and ITO/Zn_2Pc_2/C60/Al were fabricated. The effect of the thickness of the active Pc layer – the thickness of the Pc layer was varied from 15 to 80 nm – on solar cells parameters has been investigated. A nearly thickness independent open circuit voltage was observed in both structures. The maximum photovoltaic conversion efficiency, short circuit current and fill factor were observed in ITO/Zn_2Pc_2/C60/Al cell with 80 nm Pc layer to be 0.255%, 1 mA cm^{-2} and 0.38, respectively. The redox properties of the ball-type complexes were investigated by cyclic voltammetry, controlled-potential coulometry and *in situ* spectroelectrochemistry in DMSO–TBAP. The electrochemical measurements showed that the complexes form ring-based and/or metal-based mixed-valence species, due to the remarkable intramolecular interactions between the two metal phthalocyanine units. The Vulcan XC-72 (VC)/Nafion(Nf)/Co_2Pc_2 modified glassy carbon electrode showed much higher catalytic performance towards oxygen reduction, compared to the VC/Nf/Zn_2Pc_2 modified one. It was found that the VC/Nf/Co_2Pc_2 catalyst is nearly insensitive to the presence of methanol. In the presence of 1 M methanol in the electrolyte, the catalytic performance of the Co_2Pc_2-based catalyst in oxygen reduction was much better than that of the Pt-based one. Thus, it was shown that the VC/Nf/Co_2Pc_2 catalyst can be a good alternative to VC/Nf/Pt as a cathode catalyst in direct methanol fuel cells.

Introduction

Ball-type phthalocyanines (Pcs) are a new class of compounds in which two Pcs monomers arranged cofacially are bridged with four substituents on the peripheral positions of the benzene rings. The first synthesis of a ball-type Pc was reported in 2002.[1,2] The results of our previous studies suggested that these compounds usually display interesting electrical,[3–5] electrochemical,[6] gas sensing[7] and optical properties,[8] due to strong intramolecular interactions between the two face to face Pc rings and/or metal centers. Therefore, this new class of compounds have advantages in their applications in various fields of technology such as fuel cells, optoelectronics, semiconductors and sensors, over the common mononuclear and non-interacting dinuclear Pcs. For instance, ball-type cobalt phthalocyanines displayed high catalytic activity towards dioxygen reduction, which has vital importance in fuel cell applications.[9,10] In most cases, their high catalytic activities were attributed to the presence of two interacting redox-active metal centers, coordinating ability of these metal centers for dioxygen and the suitable distance between the two MPc units. In this respect, the comparison of the various physicochemical properties of ball-type Pcs involving redox-active metal centers such as Co(II) or Fe(II) with the others including redox-inactive metal centers such as Cu(II) or Zn(II) is useful in identifying and explaining the reason for their extraordinary properties.

The fact that the nature of the metal centers and the bridging substituents lead to important changes in ball-type Pc characteristics and our continuing efforts in the design of novel macrocycles with potential applicability in various technological areas prompted us to synthesize new examples of this type of compounds with dicumarol bridging units and different metal centers. For a long time, binuclear Pcs have been obtained by

[a]*Department of Chemistry, Marmara University, 34722 Kadıköy, İstanbul, Turkey. E-mail: usalan@marmara.edu.tr, aliozkaya@marmara.edu.tr; Fax: +90 216 347 87 83; Tel: +90 216 347 96 41*
[b]*Physics Department, Yıldız Technical University, 34212 Davutpaşa, İstanbul, Turkey. E-mail: altindal@yildiz.edu.tr*
[c]*Chemistry Department, Hacettepe University, 06532 Beytepe, Ankara, Turkey. E-mail: bekir@hacettepe.edu.tr*
[d]*Department of Chemistry, Istanbul Technical University, 34469 Maslak, Istanbul, Turkey. E-mail: obek@itu.edu.tr*

†Electronic supplementary information (ESI) available: absorption spectra of compounds **4** and **5** in DMSO and ^{1}H-NMR spectrum of compound **5** in DMF. See DOI: 10.1039/c2dt12510b

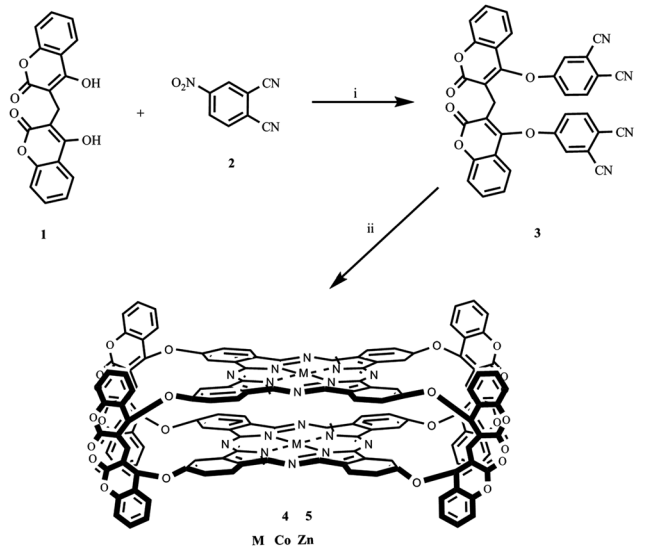

Scheme 1 (i) K_2CO_3, DMSO; (ii) **4**/$Co(OAc)_2{\cdot}4H_2O$, 300 °C; **5**/$Zn(OAc)_2{\cdot}2H_2O$, 300 °C.

the tetramerization of phthalonitrile (or its derivatives) with basic catalysts in a suitable solvent such as hexanol, pentanol or dimethylformamide (DMF) at 180–200 °C. Recently researchers have used new techniques such as 'microwave irradiation' or 'heating of the solid phase' to synthesize binuclear Pcs.

In this paper, we have used the 'heating of the solid phase' method for the synthesis of novel ball-type Co^{II} **4** and Zn^{II} **5** Pcs. Our starting compound 4,4′-bis(dicoumaroylphthalo-nitrile) **3** was synthesized from the reaction of 3,3′-methylenebis(4-hydroxy-2*H*-chromen-2-one) **1** and 4-nitrophthalonitrile **2**, in dry dimethylsulfoxide (DMSO) in the presence of dry K_2CO_3. Complexes **4** and **5** were prepared by heating **3** with excess $Co(OAc)_2{\cdot}4H_2O$ and $Zn(OAc)_2{\cdot}4H_2O$ in a N_2 atmosphere in a sealed tube (Scheme 1).

Results and discussion

In this study, a novel compound 4,4′-bis(dicoumaroylphthalonitrile) **3** was prepared and used as a key compound for the preparation of new ball-type metallo bisphthalocyanines (Co_2Pc_2 **4** and Zn_2Pc_2 **5**) which were achieved by the reaction of 3,3′-methylenebis(4-hydroxy-2*H*-chromen-2-one) **1** and 4-nitrophthalonitrile **2**, in dry DMSO in the presence of K_2CO_3, in a 67% yield. The resulting compounds were purified by washing with hot acetic acid and ethanol, respectively, using Soxhlet apparatus and column chromatography. Melting points of the Pcs were found to be higher than 350 °C.

Elemental analysis, IR, ^{1}H NMR, MALDI-TOF mass and UV/Vis spectra confirmed the proposed structures of the compounds. A diagnostic feature of Pcs formation from compound **3** was the disappearance of the sharp intense CN vibration band at 2231 cm^{-1} in the IR spectrum. The IR spectra taken with KBr pellets showed Ar–O–Ar peaks at 1242–1251 cm^{-1}, an aromatic C═C peak at around 1517–1602 cm^{-1}, C═O peaks at 1717–1770 cm^{-1}, an aromatic CH peak at 3044–3054 cm^{-1}, and an aliphatic CH_2 at 2848–2940 cm^{-1} for the compounds **4** and **5**.

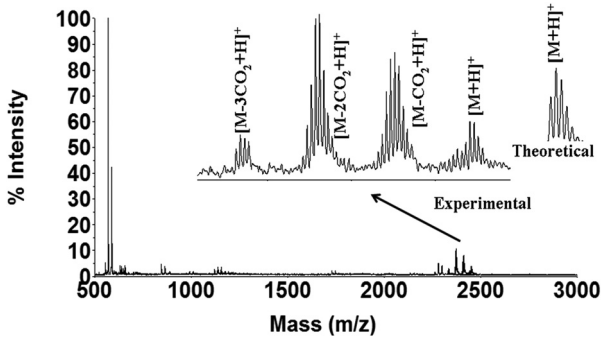

Fig. 1 A positive ion reflectron mode MALDI-TOF mass spectrum of **4** in α-cyano-4-hydroxycinnamic acid MALDI matrix using a nitrogen laser (at 337 nm wavelength) accumulating 100 laser shots. Insets show the experimental and theoretical isotopic mass distributions of the protonated molecular ion.

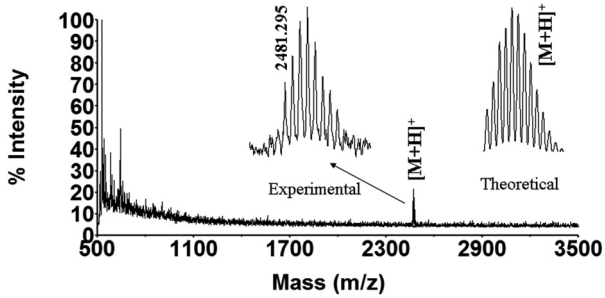

Fig. 2 A positive ion reflectron mode MALDI-TOF mass spectrum of **5** in α-cyano-4-hydroxycinnamic acid MALDI matrix using a nitrogen laser (at 337 nm wavelength) accumulating 100 laser shots. Insets show the experimental and theoretical isotopic mass distributions of the protonated molecular ion.

Electronic spectra are especially fruitful in establishing the structure of ball type metallo bisphthalocyanines **4** and **5** (ESI, Fig. S1†). The Q band observed for the compounds was attributed to the $\pi \rightarrow \pi^*$ transition from the highest occupied molecular orbital (HOMO) to the lowest unoccupied molecular orbital (LUMO) of the Pc ring. The B bands in the UV region were observed due to the transitions from deeper π levels to the LUMO. The UV/Vis spectra of **4** and **5** exhibited the intense Q bands at 675, 685 nm and 701, 684 nm, respectively. As expected, good splitting of the Q bands in the spectra of **4** and **5** were observed. This can be attributed to strong intramolecular interactions between the Pc rings, probably due to the ball-type cofacial structure. ^{1}H NMR spectra were also in good correlation with the structure of the synthesized compounds (ESI, Fig. S2†).

In the ^{1}H NMR spectrum of compound **3**, which was taken in d-chloroform, the phenyl protons appeared at 7.36 ppm (t), 7.37 ppm (d), 7.58 ppm (br t), 8.00 ppm (dd), 8.08 ppm (d), 8.59 ppm (dd), 8.66 ppm (d), and $-CH_2$ protons at 3.85 ppm (s). Aromatic protons of **5** appeared as multiples at 6.80–7.80 ppm in its ^{1}H NMR spectrum.

Positive ion and reflectron mode MALDI-TOF mass spectra of the complexes are shown in Figs 1 and 2. Some commercial MALDI matrices were tried to find an intense molecular ion signal and low fragmentation under MALDI-TOF mass

spectrometry conditions for these compounds. Mainly complexes were yielded at high intensity protonated ion signals in α-cyano-4-hydroxycinnamic acid MALDI matrix. Protonated ion signals of **4** were observed at reasonable high intensity in reflectron mode, protonated ion signals were observed at reasonably high intensity in reflectron mode, and followed at least three CO_2 elimination fragments. For both complexes, the theoretical and experimental isotopic mass distribution of the protonated molecular ion peaks were compared (the insets in Figs 1 and 2). It was noticed that the experimental and theoretical isotopic peak distributions completely matched each other for each complex. This shows that all compounds were synthesized successfully using the synthesis route given in the Experimental section.

The characterization of the fabricated solar cells was carried out in ambient air under an illumination of 100 mW cm^{-2} with an AM1.5G sun simulator. In order to characterize the roles of the thickness of the Pc layer in ITO/Pc/C60/Al cells, the thickness of the Pc layer was varied from 15 to 80 nm. The solar cell parameters such as short circuit current (I_{sc}), open circuit voltage (V_{oc}), fill factor (FF) and photovoltaic conversion efficiency (η) are the key parameters and should be determined under particular illumination conditions, the so called standard test conditions.[11] The photovoltaic conversion efficiency of a solar cell is defined as,

$$\eta = (V_{oc} \times I_{sc} \times FF)/P_{in} \quad (1)$$

where FF is given by,

$$FF = (I_{max} \times V_{max})/(I_{sc} \times V_{oc}) \quad (2)$$

where I_{max} and V_{max} are the current and voltage at the certain point on the *I–V* characteristics in which the cell delivers the maximum power density.

Fig. 3 compares the current density *versus* voltage (*J–V*) characteristics of various cells prepared using different thicknesses of the Pc layers under 100 mW cm^{-2} illumination and the device performance parameters are summarized in Table 1 for numerical comparison. Although the open circuit voltages of all devices are about 0.67 ± 0.04 V irrespective of the thickness of the Pc layer, the short circuit current of the same cells increases dramatically with the thickness of the Pc layer. Recently, it was discussed in the literature[12,13] that the energy difference between the HOMO of the donor and the LUMO of the acceptor is closely correlated to the V_{oc} value. Therefore, a thickness independent V_{oc} is expected because the V_{oc} depends mostly on the energy levels of the donor and acceptor materials. On the other hand, there are many reports on increasing the V_{oc} by changing the thickness of the Pc layer. The effect of the CuPc layer thickness on the open circuit voltage and short circuit current in ITO/PEDOT:PSS/CuPc/Al solar cell devices was investigated by Rajaputra *et al.*[14] They concluded that the enhancement in the V_{oc} with thickness is primarily due to enhanced J_{sc} and not due to reduced reverse saturation current density. That means, by considering the previous reports on increasing of V_{oc}, there is some factor, which limits this correlation.

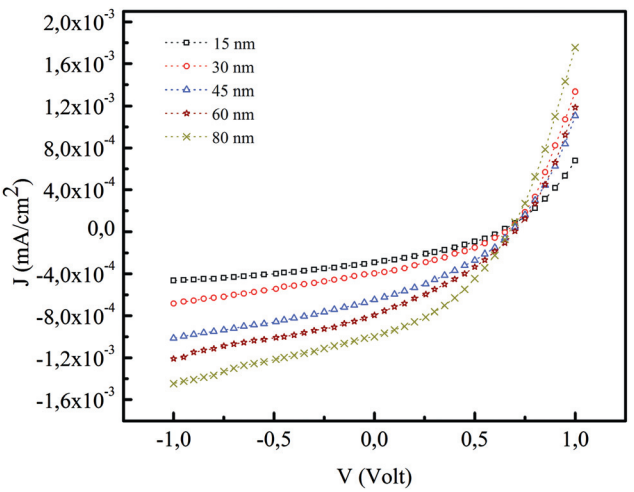

Fig. 3 *J–V* characteristics of the ITO/**5**/C_{60}/Al photovoltaic devices at different thicknesses of the film of **5**.

It should be noted that not only I_{sc} but also FF and η show a strong dependence on Pc layer thickness, the photovoltaic conversion efficiency increases with increasing Pc layer thickness reaching a value of 0.255% for a **5** layer thickness of 80 nm. The increase in I_{sc} and η with Pc layer thickness can be attributed to the following two reasons: it is well known that the Pc is a good absorber of visible light of 550–800 nm, an increase in the thickness of photoactive layer leads to greater absorption and hence more exciton generation, which in turn leads to enhanced photovoltaic performance. It is well established that the structural arrangement and the overlap of the π-electron systems between the neighbour molecules in the thin film play a fundamental role in the electrical and optical properties of Pc compounds. Therefore, another possible reason for the improved photovoltaic performance in the thicker active layer is the change in the degree of crystallinity, grain size and stacking arrangement of the Pc molecules with increasing film thickness. Senthilarasu *et al.*[15] demonstrated how the film thickness rearranges the molecular stacks. They observed that the degree of crystallinity and grain size increase with the film thickness. The increase in the degree of crystallinity and grain size may result in altering the interaction of the π-electron systems between the different molecules, which may affect the photovoltaic performance of the cells. The comparison of the performance parameters of ITO/**5**/C60/Al and ITO/**4**/C60/Al in which the thicknesses of the Pc layers were varied from 15 to 80 nm for both devices, indicates that ITO/**5**/C60/Al structure has better photovoltaic performance than ITO/**4**/C60/Al for all thicknesses of Pc layer.

The redox properties of **4** and **5** were examined by cyclic voltammetry and controlled-potential coulometry (CPC) in DMSO–TBAP (tetrabutylammonium perchlorate). A typical cyclic voltammogram for **5** at 0.050 V s^{-1} is shown in Fig. 4A. It displayed four reductions at $E_{1/2}$ = −0.64 V (R1), $E_{1/2}$ = −0.99 V (R2), $E_{1/2}$ = −1.31 V (R3) and $E_{1/2}$ = −1.7 V (R4) and an

Table 1 The effect of the thickness of the Pc layer on the photovoltaic performance of ITO/**5**/C_{60}/Al and ITO/**4**/C_{60}/Al devices

Thickness (nm)	I_{sc} (mA cm^{-2})	V_{oc} (V)	FF	η (%)
15	0.30/0.12	0.63/0.64	0.33/0.20	0.062/0.047
30	0.40/0.18	0.66/0.65	0.33/0.18	0.087/0.062
45	0.65/0.28	0.68/0.65	0.34/0.17	0.150/0.088
60	0.80/0.45	0.70/0.71	0.33/0.19	0.185/0.107
80	1.00/0.53	0.67/0.68	0.38/0.23	0.255/0.104

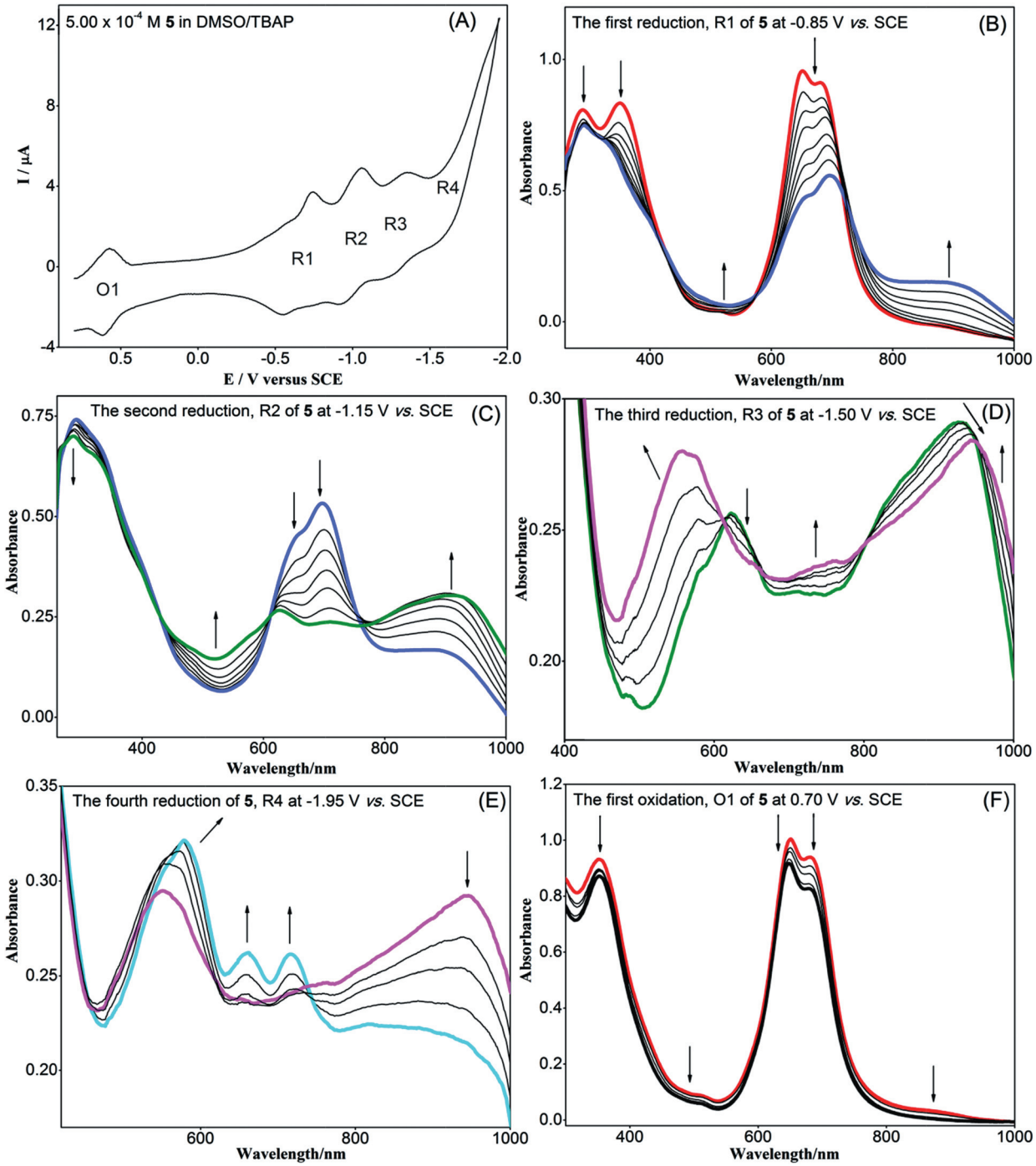

Fig. 4 A cyclic voltammogram of 5.00×10^{-4} M **5** at 0.100 V s^{-1} (A) and *in situ* UV/Vis spectral changes monitored during its first reduction at −0.85 V (B), second reduction at −1.15 V (C), third reduction at −1.50 V (D), fourth reduction at −1.95 V (E) and *first* oxidation at 0.70 V *vs.* SCE (F) on Pt in DMSO–TBAP.

oxidation at $E_{1/2}$ = 0.60 V *vs.* saturated calomel electrode (SCE) (O1) in DMSO–TBAP. The CPC studies showed that each broadly separated redox process involves the transfer of one electron. The transfer of one electron in each redox process suggests that the reduction or oxidation of each ZnPc unit in dinuclear ball-type **5** occurs at a different potential, as a result of the interaction between the two cofacial ZnPc units and thus, the splitting of the molecular orbitals. It is clear from the previous studies that the Zn^{II} metal center is not redox-active in metallo Pcs and thus, all redox processes of **5** are ligand-based.[16,17] As illustrated schematically in Chart 1, these processes are associated with the presence of mixed-valence species, $[Zn^{II}Pc(-2)\cdot Zn^{II}Pc(-1)]^{+}$, $[Zn^{II}Pc(-2)\cdot Zn^{II}Pc(-3)]^{-}$ and $[Zn^{II}Pc(-3)\cdot Zn^{II}Pc(-4)]^{3-}$.

The splitting of a redox process *i.e.*, Pc(−2)/Pc(−3), for **5**, due to formation of a stable mixed-valence intermediate, $[Zn^{II}Pc(-2)\cdot Zn^{II}Pc(-3)]^{-}$, is a measure of the equilibrium

$$[Zn^{II}Pc(-1)Zn^{II}Pc(-2)]^{+} \overset{e^-}{\rightleftharpoons}_{O1} [Zn^{II}Pc(-2)]_2 \overset{e^-}{\rightleftharpoons}_{R1} [Zn^{II}Pc(-3)Zn^{II}Pc(-2)]^{-} \overset{e^-}{\rightleftharpoons}_{R2} [Zn^{II}Pc(-3)]_2^{2-}$$

$$[Zn^{II}Pc(-3)]_2^{2-} \overset{e^-}{\rightleftharpoons}_{R3} [Zn^{II}Pc(-3)Zn^{II}Pc(-4)]^{3-} \overset{e^-}{\rightleftharpoons}_{R4} [Zn^{II}Pc(-4)]_2^{4-}$$

Chart 1 Electrode reactions for **5**.

(comproportionation) constant, K_c, for a reaction such as:[16]

$$[Zn^{II}Pc(-3)]_2^{2-} + [Zn^{II}Pc(-2)]_2 \rightleftharpoons 2[Zn^{II}Pc(-2)] \cdot [Zn^{II}Pc(-3)]^{-}$$

where the mixed-valence splitting, ΔE_s is related to K_c, *via*:

$$\Delta E_s = (RT/nF)\ln K_c \quad (3)$$

The mixed-valence splitting energy, ΔE_s, values of Pc(−2)/Pc(−3) and Pc(−3)/Pc(−4) redox processes, *i.e.*, the difference between the half-peak potentials of R1 and R2, and R3 and R4, respectively, in **5** are 0.35 and 0.39 V, respectively, indicating remarkable stability of the relevant mixed-valence species. The values of K_c obtained for the mixed-valence species of **5**, $[Zn^{II}Pc(-2)\cdot Zn^{II}Pc(-3)]^{-}$ and $[Zn^{II}Pc(-3)\cdot Zn^{II}Pc(-4)]^{3-}$, are 8.55×10^5 and 4.08×10^6, respectively. The high K_c and ΔE_s values of **5** give evidence of the delocalization of charge among the cofacial Pc units, and thus the formation of electrochemically reduced mixed-valence species.

In situ spectroelectrochemical measurements enabled us to monitor the UV/Vis spectra of electrochemically reduced species of **5** (Fig. 4B–E). The decrease in the split Q band with the red shift of the one at 680 nm to 697 nm during the first reduction process, R1, and to 715 nm during the second reduction process, R2, and the one at 651 nm to 625 nm during the second reduction process R2 is accompanied by the increase in the absorption between 500–600 nm and the formation of a new band around 900 nm (Fig. 4B and C). These spectral changes, especially the increase in the absorption between 500–600 nm, are characteristic for ring reduction. However, in general, the shift in the Q band is not observed during ring reductions of mono metallo Pcs including a redox inactive metal center. The shifts observed here should be due to the changes in the intramolecular interactions between the two Pc rings in ball-type **4**, upon reduction. As shown in Fig. 4D and E, the formation of new intense bands at 561 and 579 nm during the third and fourth reduction processes confirm the ring-based nature of these processes and thus, the formation of $[Zn^{II}Pc(-3)ZnPc(-4)]^{3-}$ and $[Zn^{II}Pc(-4)]_2^{4-}$ species, respectively. Unfortunately, singly oxidized $[Zn^{II}Pc(-2)\cdot Zn^{II}Pc(-1)]^{+}$ species could not be obtained during the constant-potential electrolysis at 0.70 V *vs.* SCE (Fig. 4F) although a well-defined redox couple was obtained during cyclic voltammetry measurements (Fig. 4A). As shown in Fig. 4F, the absorption of the all bands decreases during the electrolysis and isosbestic points are not observed which implies that under the conditions of constant-potential electrolysis, decomposition of the complex occurs.

A typical cyclic voltammogram of **4** in TBAP–DMSO is shown in Fig. 5. It displays two quasi-reversible oxidations at $E_{1/2}$ = 0.07 V (O1) and $E_{1/2}$ = 0.60 V *vs.* SCE (O2) and three

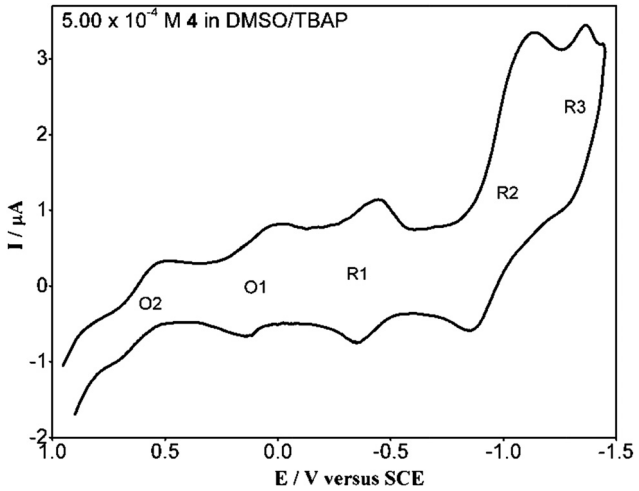

Fig. 5 A cyclic voltammogram of **4** at 0.050 V s^{-1} on Pt in DMSO–TBAP.

reversible or quasi-reversible reductions at $E_{1/2}$ = −0.39 V (R1), $E_{1/2}$ = −0.99 V (R2) and $E_{1/2}$ = −1.33 V *vs.* SCE (R3). CPC measurements and anodic to cathodic peak separations in the cyclic voltammogram suggested that all redox couples are one-electron reversible or quasi-reversible processes except the second reduction couple, R2 which involves the transfer of two electrons per molecule. The transfer of one electron in each of the broadly separated O1 and O2 steps implies that the oxidation of each MPc ring of **4** occurs at different potentials as stepwise one-electron redox couples of the two cofacial Pc units, as a result of the interaction between them and thus, the splitting of the molecular orbitals. The metal centre in a Co^{II} phthalocyanine is redox-active due to the presence of d orbital levels within the HOMO–LUMO gap.[4,16,17] Depending on its environment in solution, the electrochemistry of cobalt Pcs is split into two sections, that referring to donor solvents and that referring to non-donor solvents. The main difference lies in whether metal or the ring is oxidized first. Donor solvents strongly favour the oxidation of Co^{II} to Co^{III} by coordinating along the axis to form six coordinate species. If such donor solvents are absent, then oxidation to Co^{III} is inhibited and ring oxidation occurs first. On the other hand, the first reduction process is metal-based both in donor and nondonor solvents. Thus, the first and the second oxidation processes of **4** are probably metal-based and correspond to $[Co^{II}Pc(-2)]_2/[Co^{III}Pc(-2)\cdot Co^{II}Pc(-2)]^{+}$ and $[Co^{II}Pc(-2)\cdot Co^{III}Pc(-2)]^{+}/[Co^{III}Pc(-2)]_2^{2+}$ redox processes, respectively, since each molecule of ball-type **4** involves two Co^{II} centers and the voltammetric measurements were carried out in DMSO–TBAP. *In situ* UV/Vis spectroelectrochemical measurements in DMSO–TBAP were also carried out to confirm the assignment of the redox processes.

Fig. 6A shows the spectral changes recorded during the first oxidation process of **4**. The Q band in the spectrum monitored at the beginning of the electrolysis is considerably broad, probably due to the intra molecular interactions between the two MPc units in **4**. An alternative or additional reason for the broad Q band may be the presence of aggregated species at high concentrations used in the optically transparent thin layer electrode (OTTLE) cell. The red shift in the Q band from 670 nm to

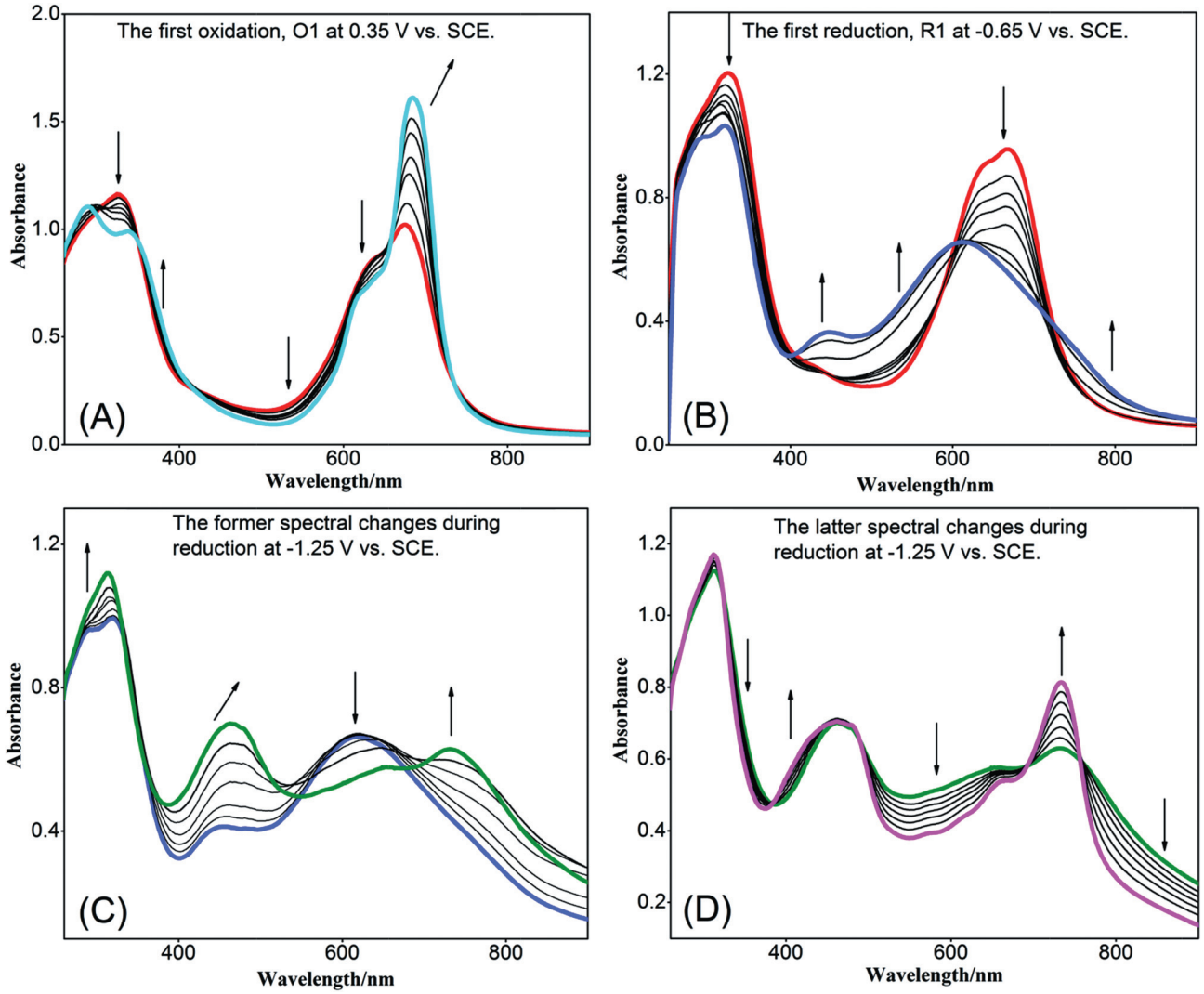

Fig. 6 *In situ* UV/Vis spectral changes monitored during the redox processes of **4** in TBAP–DMSO.

680 nm confirms the assignment of the first oxidation couple to $[Co^{II}Pc(-2)]_2/[Co^{II}Pc(-2)\cdot Co^{III}Pc(-2)]^+$. However, during the electrolysis at 0.80 V *vs.* SCE, the absorptions of the all bands decreased suggesting decomposition of the complex although a well-defined second oxidation couple, O2 was observed in its cyclic voltammogram. The one-electron quasi-reversible first reduction of **4**, R1, can be attributed to $[Co^{II}Pc(-2)]_2/[Co^{II}Pc(-2)\cdot Co^{I}Pc(-2)]^-$, as evidenced by the spectral changes observed during the electrolysis at −0.65 V *vs.* SCE. As shown in Fig. 6B, the absorption of the Q band decreases with blue shift to 613 nm which is associated with the formation of a new band at 442 nm. These spectral changes confirm the formation of $Co^{II}\cdot Co^{I}$ mixed-valence species.[18,19] It is known from the literature[20,21] that both $Co^{II}\cdot Co^{I}$ and $Co^{I}\cdot Co^{I}$ species show Q band and metal-to-ligand charge transfer (MLCT). The new band at 442 nm can be assigned to MLCT from Co^{I} to the Pc ring. During the reduction at −1.25 V *vs.* SCE, two groups of spectral changes are observed with different isosbestic points (Fig. 6C and D). At the beginning, the Q band at 613 nm decreases with red shift and nearly disappears while a new band at 734 nm forms and the band at 442 nm increases with red shift to 464 nm (Fig. 6C). These spectral changes indicate the formation of $Co^{I}\cdot Co^{I}$ species. The MLCT from Co^{I} to the Pc ring is observed around 473 nm in the case of mono cobalt Pcs. The former spectral changes are followed by an increase without shift in the band at 734 nm and a decrease in the absorption around 600 nm (Fig. 6D). These latter spectral changes are characteristic for ring reduction and should correspond to the reduction of one of the Pc rings in **4**. The occurrence of two groups of spectral changes with different isosbestic points at −1.25 V *vs.* SCE and the transfer of two electrons per molecule during the R2 process show that the second metal center reduction and the first ring reduction of **4** are merge into one redox couple. Thus, R2 and R3 couples of **4** can be assigned to $[Co^{II}Pc(-2)\cdot Co^{I}Pc(-2)]^-/[Co^{I}Pc(-2)\cdot Co^{I}Pc(-3)]^{3-}$ and $[Co^{I}Pc(-2)\cdot Co^{I}Pc(-3)]^{3-}/[Co^{I}Pc(-4)]^{4-}$. The voltammetric electrode reactions and mixed-valence species produced electrochemically as a result of the redox processes of dimeric ball-type **4** are schematically illustrated in Chart 2.

The splitting of the Co^{II}/Co^{III} redox process in **4**, due to formation of the stable mixed-valence intermediate,

$$[Co^{III}Pc(-2)]_2^{2+} \underset{O2}{\overset{e^-}{\rightleftharpoons}} [Co^{III}Pc(-2).Co^{II}Pc(-2)]^{+} \underset{O1}{\overset{e^-}{\rightleftharpoons}} [Co^{II}Pc(-2)]_2 \underset{R1}{\overset{e^-}{\rightleftharpoons}} [Co^{II}Pc(-2)Co^{I}Pc(-2)]^{-}$$

$$[Co^{II}Pc(-2)Co^{I}Pc(-2)]^{-} \underset{R2}{\overset{2e^-}{\rightleftharpoons}} [Co^{I}Pc(-2).Co^{I}Pc(-3)]^{3-} \underset{R3}{\overset{e^-}{\rightleftharpoons}} [Co^{I}Pc(-3)]_2^{4-}$$

Chart 2 Electrode reactions for **4**.

$[Co^{III}Pc(-2)\cdot Co^{II}Pc(-2)]^{+}$, is a measure of the equilibrium (comproportionation) constant, K_c, for the reaction:

$$[Co^{III}Pc(-2)]_2^{2+} + [Co^{III}Pc(-2)]_2 \rightleftharpoons [Co^{III}Pc(-2)\cdot Co^{II}Pc(-2)]^{+}$$

The mixed-valence splitting energy, ΔE_s, of Co^{II}/Co^{III} redox process for **4**, *i.e.*, the difference between the half-peak potentials of O1 and O2 couples is 0.53 V which leads to K_c value of 9.61×10^8, suggesting high stability of the mixed-valence species of $[Co^{III}Pc(-2)\cdot Co^{II}Pc(-2)]^{+}$. The difference between the stepwise reduction potentials of **4** is remarkably high, which indicates that the mixed-valence species of $[Co^{II}Pc(-2)Co^{I}Pc(-2)]^{-}$ and $[Co^{I}Pc(-2)\cdot Co^{I}Pc(-3)]^{3-}$ are considerably stable. However, it is not suitable to determine the relevant comproportionation constants due to the coalescence of second and third reduction redox couples.

Some recent reports of our group suggested that electrocatalytic performances of ball-type dinuclear metallo Pcs with cyclopentyldisilanoxy-polyhedral oligomeric silsesquioxanes,[9] perfluorodecyl,[22] pentaerythritol,[10] 1,1′-methylenedinaphthalen-2-ol[23] and dithioerythritol[24] bridging units towards the oxygen reduction reaction (ORR) are encouraging for applicability in fuel cells. For this reason, the electrocatalytic performance of the ball-type Pc complexes **4** and **5** towards ORR was tested by the ring and disk polarization curves of a rotating ring disk electrode (RRDE), modified by a mixture of the relevant Pc complex with Vulcan XC-72 (VC) and Nafion (Nf), in O_2-saturated 0.5 M H_2SO_4 aqueous electrolyte solution (Fig. 7A). The onset potential (E_o) where the oxygen reduction current begins to increase, the limiting diffusion disk current density (J_L) and the half-wave potential ($E_{1/2}$) for the ORR were taken as the measures of catalytic performance. The disk potential at which the current density reaches 0.100 mA cm^{-2} was taken as E_o. Table 2 summarizes the electrocatalytic performances of **4** and **5**, in comparison with previously reported ball-type cyclopentyldisilanoxy-polyhedral oligomeric silsesquioxanes-,[9] pentaerythritol-[10] and dithioerythritol-bridged[24] binuclear metallo Pcs. Contrary to **5**, complex **4** displays two reduction waves, well-separated from each other. The limiting current for the first wave implies that the ORR probably occurs *via* peroxo species, producing water as the main product and some hydrogen peroxide as the side product. The second wave, appearing at considerably negative potentials presumably corresponds to the reduction of hydrogen peroxide to water. The absolute ring current decreases simultaneously while the disk current increases during the appearance of the second wave (Fig. 7A), which confirms that hydrogen peroxide produced at the first step as the side product is further reduced to water during the second wave. The ORR occurs at much more positive potentials at the VC/Nf/**4** modified GCE than that at the VC/Nf/**5** modified one. In addition, the limit current density for the VC/Nf/**4** modified GCE is much higher than that of VC/Nf/**5** modified one. These findings clearly indicate the higher catalytic activity of the former relatively.

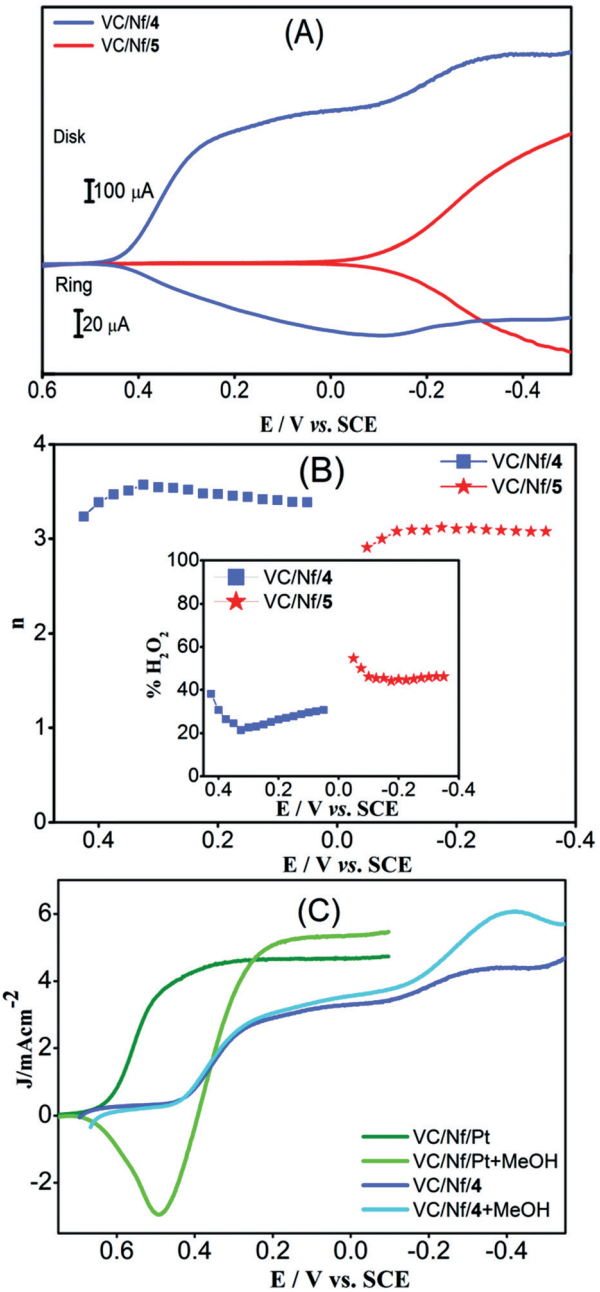

Fig. 7 (A) RRDE polarization curves for the electrocatalytic ORR at 0.005 V s^{-1} on a VC/Nf/M_2Pc_2 modified rotating (2500 rpm) glassy carbon disk electrode and platinum ring electrode in O_2-saturated 0.5 M H_2SO_4. (B) The number of total electrons exchanged for VC/Nf/M_2Pc_2 modified electrodes (inset shows $\%H_2O_2$ produced in the ORR as a function of disk potential (E_{ring} = 0.95 V *vs.* SCE)). (C) RDE polarization curves for the electrocatalytic ORR at 0.005 V s^{-1} on VC/Nf/Pt and VC/Nf/**4** modified rotating (2500 rpm) glassy carbon electrodes in the presence and absence of 1 M methanol in O_2-saturated 0.5 M H_2SO_4.

The ring currents in RRDE voltammetry measurements, carried out with a VC/Nf/M2Pc2 modified glassy carbon disk

Table 2 Electrocatalytic properties of **4** and **5**, and the comparison with previously reported[9,10,24] ball-type cobalt phthalocyanine dimers

Complex	E_o for ORR[a] (V)	J_L for ORR[b] (mA cm^{-2})	$E_{1/2}$ for ORR (V)	Ref.
Zn_2Pc_2 **5**	−0.01	2.07	−0.21	tw[c]
Co_2Pc_2 **4**	0.45	2.63	0.35	tw[c]
		0.92	−0.20	
Zn_2Pc_2[d]	−0.18	0.86	−0.21	24
Co_2Pc_2[d]	0.10	3.30	−0.14	24
Co_2Pc_2[e]	0.68	4.27	0.41	9
		2.17	−0.19	
Co_2Pc_2[f]	0.25	4.50	−0.09	10
Co_2Pc_2[g]	0.61	4.84	0.05	10

[a] The potential at which the current density reaches 0.100 mA cm^{-2} was taken as the onset potential. [b] The limiting diffusion current density at 2500 rpm. [c] This work. [d] Dithioerythritol-bridged ball-type zinc and cobalt phthalocyanine. [e] Ball-type cyclopentyldisilanoxy-polyhedral oligomeric silsesquioxanes-bridged cobalt phthalocyanine. [f] Pentaerythritol-bridged ball-type cobalt phthalocyanine. [g] Pentaerythritol-bridged ball-type cobalt phthalocyanine with heptadecafluorodecyl substituents.

electrode and a platinum ring electrode polarized at 0.95 V *vs.* SCE were used to determine the number of electrons transferred, n_t, and estimate the amount of generated hydrogen peroxide and thus water selectivity since the ORR in an acidic medium can be either a four-electron process to form water or a two-electron reduction to form hydrogen peroxide (Fig. 7A). It is desirable that the ORR goes to completion and forms water *via* a four-electron transfer mechanism. However, in the case of low catalytic activity, oxygen gets reduced to hydrogen peroxide *via* a two-electron process, but the peroxide can still get reduced further *via* another two-electron process to form water. It can be observed that the increase in the absolute ring current initiates at the same potential as the onset potential for the ORR in both VC/Nf/**4** and VC/Nf/**5** modified disk electrodes, indicating that the generation of hydrogen peroxide is taking place (Fig. 7A). The n_t and the percentage of hydrogen peroxide produced at a given potential was determined by the following equations:[25–27]

$$n_t = 4I_D[I_D + (I_R/N)] \quad (4)$$

$$\%H_2O_2 = 100(4 - n_t)/2 \quad (5)$$

where N, I_D, and I_R are the collection efficiency, disk current and ring current, respectively. Fig. 7B shows the n_t and percentage of hydrogen peroxide and water generated at different potentials. The obtained values confirm that the ORR on the **4**-based electrode produces a higher amount of water than that of hydrogen peroxide, *i.e.*, the numbers of exchanged electrons at different potentials on the ORR wave are higher than 3 which corresponds to the formation of equal amounts of water and hydrogen peroxide. The n_t value increases with increasing overvoltage and becomes 3.58 (79% H_2O and 21% H_2O_2) first, and then decreases slightly to 3.38 (69% H_2O and 31% H_2O_2) at the limiting diffusion current plateau, leading to the production of water as the main product. The detection of hydrogen peroxide suggests that the first step of the series path, *i.e.*, oxygen reduction to hydrogen peroxide is certainly operative. However, a direct path, *i.e.*, oxygen reduction to water *via* a four-electron process without the formation of hydrogen peroxide as an intermediate is the main reaction to occur. The RRDE voltammetry results showed that contrary to the **4**-based catalyst, the reduction wave of the VC/Nf/**5** modified electrode produces approximately equal amounts of water and hydrogen peroxide. At the potentials between −0.050 and −0.35 V *vs.* SCE, the n_t takes values within the range of 2.90–3.10 (45% H_2O–55% H_2O_2). Thus, water selectivity of **4** in the ORR is higher than that of **5**. Moreover, for the ORR, the overpotential of the VC/Nf/**4** modified electrode is considerably low, in comparison with that of the VC/Nf/**5** modified electrode. According to some authors,[28,29] electrocatalytic reduction of oxygen on metallo Pcs takes place through a redox-catalysis type of process where oxygen binding ability and the redox potential of the central metal ions play a critical role. The metal ion in the center of Pc ring is oxidized by oxygen molecule during its adsorption and thus reduces it. The metal center in **5** is redox-inactive, and thus neither oxidized nor reduced under the conditions of electrocatalytic measurement, as judged from their well described electrochemical behaviour.[16] On the other hand, in the case of **4**, the presence of two redox-active face-to-face metal centers promotes its interaction with O_2 molecules, the O–O bond breakage, the formation of suitable intermediates and thus reduction to water, as a result of the partial electron transfer from the filled d orbitals of the metal to the empty or partially filled π* orbitals of oxygen.[30–34] As shown in Table 2, the catalytic performance of **4** is better than those of previously reported ball-type pentaerythritol-,[10] and dithioerythritol-bridged[24] cobalt phthalocyanines whereas it is relatively low in comparison with the cyclopentyldisilanoxy-polyhedral oligomeric silsesquioxanes-bridged one,[9] especially in terms of onset and half-wave potentials for the ORR.

In a direct methanol fuel cell (DMFC), methanol can diffuse from the anode to the cathode and the performance of the fuel cell becomes impaired when the cathode contains Pt. However, metal N_4 chelates are known to be selective catalysts and, more particularly, to be tolerant to the presence of methanol during the ORR.[35–39] The methanol tolerance of a **4**-based catalyst was also determined and compared with that of platinum. Fig. 7C shows rotating disk electrode (RDE) polarization curves obtained in O_2-saturated electrolyte in the presence and absence of methanol (1.0 M) for Pt- and **4**-based catalysts. Indeed, the **4**-based electrode, especially its first reduction wave is completely insensitive towards methanol. The limiting current of the first wave is also completely independent of methanol presence. Contrary to **4**-based electrode, the polarization curve of the ORR on the Pt-based electrode is strongly affected by the presence of 1.0 M methanol in the electrolyte. The presence of 1.0 M methanol leads to a shift of the platinum catalyzed oxygen reduction potentials of 260 mV towards lower (more negative) potentials. A significant methanol oxidation current is observed over a wide range of potentials, and the catalytic activity of the Pt-based catalyst for the ORR is completely blockaded by methanol over the potential range of 0.38–0.70 V *vs.* SCE. Thus, until the potential reaches 0.40 V, the ORR on the **4**-based catalyst occurs at more positive potentials in the presence of methanol, as compared to the Pt-based one. On the basis of this result, a **4**-based catalyst can function as an alternative to Pt-based catalysts for the ORR in DMFC applications.

Experimental section

All reagents and solvents obtained from commercial suppliers were of reagent grade quality. The solvents were stored over molecular sieves (4 Å). 3,3′-Methylenebis(4-hydroxy-2*H*-chromen-2-one) **1** was used as commercially supplied. IR spectra were recorded on a Schimadzu FT-IR-8300 spectrophotometer as KBr pellets. Electronic spectra were recorded on a Schimadzu UV-1601 spectrophotometer. Elemental analyses were performed by the Instrumental Analysis laboratory of Tübitak-Ankara. ^{1}H NMR spectra were recorded with a Mercury-Vx 400 MHz instrument. Mass spectra were acquired on a Voyager-DE^{TM} PRO MALDI-TOF mass spectrometer (Applied Biosystems, USA) equipped with a nitrogen UV-Laser operating at 337 nm. Spectra were recorded in reflectron mode with an average of 100 shots.

The MALDI matrix α-cyano-4-hydroxycinnamic acid was prepared in acetonitrile–water (1 : 1, v/v) containing 0.1% trifluoroacetic acid at a concentration of 10 mg mL^{-1}. MALDI samples were prepared by mixing sample solutions (1.0 mg mL^{-1} in methanol) with the matrix solution (1 : 10, v/v) in a 0.5 mL Eppendorf® micro tube. Finally, 0.5 μL of this mixture was deposited on the sample plate, dried at room temperature and then analyzed.

The electrochemical measurements were carried out with a Princeton Applied Research Model VersoStat II potentiostat/galvanostat controlled by an external PC and utilizing a three electrode configuration at 25 °C. A platinum disk, a platinum spiral wire and a SCE served as the working, the counter and the reference electrodes, for cyclic voltammetry measurements. The reference electrode was separated from the bulk of the solution by a double bridge. Electrochemical grade TBAP in extra pure DMSO was employed as the supporting electrolyte at a concentration of 0.10 M. High purity N_2 was used for deoxygenating the solution at least 20 min prior to each run and to maintain a nitrogen blanket during the measurements. For CPC studies, Pt gauze working electrode (10.5 cm^2 surface area), Pt wire counter electrode separated by a glass bridge, and SCE as a reference electrode were used. *In situ* spectroelectrochemical measurements were carried out by an Agilent Model 8453 diode array spectrophotometer equipped with the potentiostat/galvanostat and utilizing an OTTLE cell with three-electrode configuration at 25 °C. The working electrode was transparent Pt gauze. Pt wire counter electrode and a SCE reference electrode separated from the bulk of the solution by a double bridge were used.

Ultra pure water and sulfuric acid were used to prepare the electrolyte solution in electrocatalytic measurements. VC (Cabot Co.), 5% Nf solution (Aldrich), extra pure ethyl alcohol (Merck), VC supported platinum particles (ElectroChem, Inc.) and Pc compounds were used in catalyst preparation. Glassy carbon disk electrode, platinum ring-glassy carbon disk electrode and a polishing kid for these electrodes were purchased from Pine Instruments. RDE voltammetry measurements were carried out using a Gamry Reference 600 potentiostat/galvanostat controlled by an external PC and utilizing a three-electrode configuration at 25 °C. Two Gamry Reference 600 potentiostats were connected as a bipotentiostat to control the ring and disk potentials and to collect the respective currents during RRDE experiments. A Pine Instrument Company AFMSRCE modulator speed rotator was employed in RDE and RRDE experiments. RDE measurements were performed with a glassy carbon disk (5 mm dia) in O_2 saturated 0.5 M H_2SO_4 aqueous solution under quasi-stationary conditions (0.005 V s^{-1} sweep rate) at 25 °C. For RRDE experiments, the working electrode was a glassy carbon disk (5.61 mm dia) and a platinum ring leading to a collection efficiency, N = 37%. These experiments were carried out at 2500 rpm in oxygen saturated 0.5 M H_2SO_4 aqueous electrolyte solution at 25 °C. The disk potential was swept at 0.005 V s^{-1} whereas the ring potential was held at 0.95 V *vs.* SCE. In order to disperse the catalysts on a carbon support for RDE and RRDE experiments, a mixture of the Pc compound, VC and 5% wt Nf solution in absolute ethanol was prepared and ultrasonically homogenized for half an hour. A given volume of this ink was deposited using a micropipette onto a freshly polished glassy carbon electrode leading to a catalyst loading of 106 μg cm^{-2}. The amount of Nf in the ink was adjusted so that the catalyst film was sufficiently thin, and thus its diffusion resistance was negligible. In order to obtain a total coverage of the glassy carbon surface, the deposited drop of ink was dried with pulsed air at ambient temperature to evaporate the solvent quickly. Each voltammogram was recorded with a freshly prepared electrode due to the possible catalyst degradation in acidic medium. The counter electrode was a Pt spiral and the reference electrode was a SCE.

[4,4′-Bis(dicoumaroylphthalonitrile)] (3)

A mixture of 3,3′-methylenebis(4-hydroxy-2*H*-chromen-2-one) 1 (0.97 g, 2.89 × 10^{-3} mol) and 4-nitrophthalonitrile **2** (1 g, 5.78 × 10^{-3} mol) in 30 mL dry DMSO was stirred at room temperature under N_2. K_2CO_3 (1.2 g, 8.70 × 10^{-3} mol) was added into the mixture over a period of 2 h. After stirring the reaction mixture for 5 days, the undissolved salt was removed by filtration. The reaction mixture was poured into water (100 mL) and stirred. The precipitate was filtered and washed with water. The residue was chromatographed by silica gel eluted with $CHCl_3$ and a gradient of $CHCl_3$–CH_3OH up to 100% CH_3OH. Yield: 1.12 g (66%). The compound is soluble in $CHCl_3$, CH_2Cl_2, THF, DMF. m.p. 235 °C; ^{1}H NMR (400 MHz, $CDCl_3$, TMS): δ 8.66 (2H, d, ^4J = 2.29 Hz, CH), 8.59 (2H, dd, $^{3,4}J$ = 8.56 and 2.25 Hz, CH), 8.08 (2H, d, ^3J = 8.56 Hz, CH), 8.00 (2H, dd, J = 7.96 and 1.00 Hz, CH), 7.58 (2H, br t, ^3J = 7.93 Hz, CH), 7.37 (2H, d, ^3J = 8.56 Hz, CH), 7.36 (2H, t, ^3J = 7.97 Hz, CH), 3.85 (2H, br s, CH_2); IR (KBr pellet) ν_{max}/cm^{-1}; 3044, 2923, 2231, 1667, 1606, 1532, 1407, 1277, 1253, 1160, 1110, 1055, 908, 852, 796, 745, 678, 638, 524 cm^{-1}; elemental analysis calcd (%) for $C_{35}H_{16}O_6N_4$; C 71.43, H 2.74, N 9.52; found: C 71.22, H 2.87, N 9.75.

[2′,10′,16′,24′-Tetrakis(dicoumaroyl)phthalocyaninato-dicobalt(II)] (4)

A mixture of compound 3 (0.200 g, 0.34 × 10^{-3} mol) and Co(OAc)$_2$·4H$_2$O (0.212 g, 0.85 × 10^{-3} mol) was powdered in a quartz crucible and heated in a sealed glass tube for 5 min under dry N_2 atmosphere at 300 °C. After cooling to room temperature, 5 mL of DMF was added to the residue to dissolve the product. The precipitate was filtered, multiply washed at first with hot

water and then with hot ethanol in order to eliminate the unreacted starting materials, and dried *in vacuo*. Then, the crude product was washed with acetic acid, ethanol for 12 h, respectively, in a Soxhlet apparatus. The residue was coarsely fractionated on a silica gel column eluting with chloroform and a gradient of chloroform–THF up to 100% THF. This blue-green compound is soluble in THF, DMF, DMSO. Yield: 110 g (13%). m.p. >350 °C; IR (KBr pellet) ν_{max}/cm^{-1}; 3044, 2940, 2850, 1770, 1717, 1589, 1520, 1463, 1404, 1242, 1088, 957, 877, 827, 748, 637, 520 cm^{-1}; UV/Vis (DMSO): $\lambda_{max}(\varepsilon)$ = 675 (4.410), 685 (4.394), 323.5 (4.337 mol^{-1} dm^3 cm^{-1}); elemental analysis calcd (%) for $C_{140}H_{64}N_{16}O_{24}Co_2$; C, 68.02; H, 2.61; Co, 4.77; N, 9.07; found: C, 68.25; H, 2.41; Co, 4.81; N, 8.87; MS (MALDI-TOF): *m*/*z* 2471 ($M + 1^+$).

[2′,10′,16′,24′-Tetrakis(dicoumaroyl)phthalocyaninato-dizinc(II)] (5)

A mixture of compound **3** (0.200 g, 0.34 × 10^{-3} mol) and Zn-$(OAc)_2{\cdot}2H_2O$ (0.186 g, 0.85 × 10^{-3} mol) was powdered in a quartz crucible and heated in a sealed glass tube for 5 min under dry N_2 atmosphere at 300 °C. After cooling to room temperature, the green reaction product was obtained, isolated and purified using the same procedure explained above for **4**. This compound is soluble in THF, DMF, DMSO. Yield: 90 mg (10.7%). m.p. >350 °C; ^{1}H NMR (400 MHz, DMF, TMS): δ 6.80–7.80 (m, 56H); 3.96 ppm (s, 8H); IR (KBr pellet) ν_{max}/cm^{-1}; 3054, 2915, 2848, 1770, 1718, 1602, 1517, 1461, 1325, 1251, 1135, 1022, 898, 841, 721, 666, 475 cm^{-1}; UV/Vis (DMSO): $\lambda_{max}(\varepsilon)$ = 701 (4.584), 684 (4.588), 513 (3.663), 285 (4.493 mol^{-1} dm^3 cm^{-1}); elemental analysis calcd (%) for $C_{140}H_{64}N_{16}O_{24}Zn_2$: C, 67.67; H, 2.60; N, 9.02; Zn, 5.26; found: C, 67.92; H, 2.45; N, 9.22; Zn, 5.15. MS (MALDI-TOF): *m*/*z* 2481 ($M + 1^+$).

The cells were fabricated on indium tin oxide (ITO) coated glass substrates with a sheet resistance of 20 Ω cm^{-2}. After masking, patterning of the bare ITO was obtained by chemical etching in diluted HCl solution. Then the ITO coated substrates were cleaned by ultrasonic treatment in acetone, isopropyl alcohol, and deionized water. After being dried by N_2 gas, ITO surfaces were treated by UV-ozone for 15 min. The organic materials used in the fabrication of solar cells were **4**, **5** and C_{60}, they were used without any purification, as donor and acceptor, respectively. The thin films of the Pcs with different thickness between 15 and 80 nm were deposited on the patterned ITO substrate by a spin coating method using DMF as solvent. Subsequently, the films were thermally annealed at 150 °C for 15 min to evaporate the solvent. Then, on the top of the Pc layer, C_{60} with thicknesses of 20 nm and 400 nm Al layers were evaporated sequentially by thermal evaporation at a pressure below 10^{-5} mbar (Edwards Auto 500). During evaporation, there was no vacuum break between organic (C_{60}) and metal (Al) deposition. An elipsometric technique was used to measure the thickness of the films. The active area of the devices was about 5 mm^2. A schematic of the device structure is shown in Fig. 8. We have investigated the change in solar cell performance, including short circuit current (I_{sc}), open circuit voltage (V_{oc}), photovoltaic conversion efficiency (η), and fill factor (FF), as a function of Pc layer thickness under AM1.5 illumination (100 mW cm^{-2}).

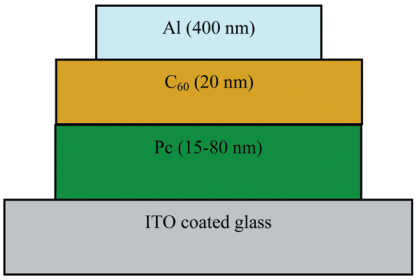

Fig. 8 A schematic diagram of the device configuration.

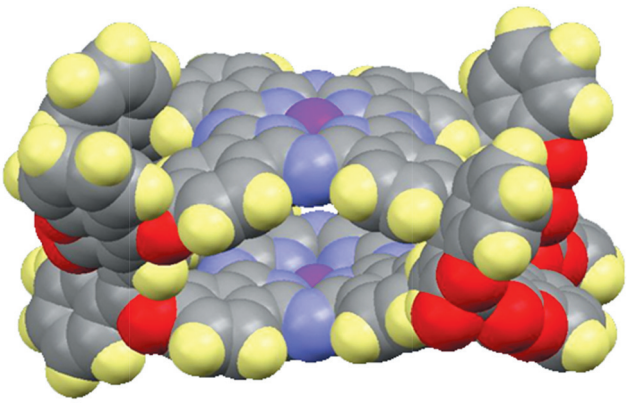

Fig. 9 The structure of the phthalocyanine compounds.

Conclusions

New ball-type Zn^{II} and Co^{II} Pcs substituted with 3,3′-methylene-bis(4-hydroxy-2*H*-chromen-2-one), **4** and **5**, were synthesized from [4,4′-bis(dicoumaroylphthalonitrile)] **3**. The complexes were characterized by elemental analysis, UV/Vis, IR, ^{1}H NMR and MALDI-TOFF mass spectroscopies. The structure of the resulting compounds was refined by performing on optimized geometry calculation in MOPAC using first AM1 then PM3 parameters (Fig. 9).[40]

A set of organic photovoltaic cells based on **4**, **5** donor molecules and C_{60} acceptor molecules has been prepared. Investigation of the effects of active layer thicknesses on the performance of the photovoltaic cells indicates that the performance parameters of the solar cells such as photovoltaic conversion efficiency, short circuit current and fill factor strongly depend on the Pc layer thickness. It was observed that the device with an 80 nm **5** layer exhibits the highest photovoltaic conversion efficiency, short circuit current and fill factor. All these findings suggest that the performance of the ITO/**5**/C_{60}/Al photovoltaic devices can be improved by the optimization of the thickness of the Pc layer. It can be said that compound **5** has a good potential for photovoltaic applications.

The electrochemical measurements of binuclear ball-type complexes **4** and **5** showed formations of electrochemically stable metal- and ligand-based mixed-valence species, due to the

intramolecular interactions between the two MPc units. The high mixed-valence splitting values for these species suggested that the interactions between the two MPc units in the complexes are remarkable. Complex **4** showed remarkable catalytic activity towards the ORR in an acidic medium, as compared to **5**. The distinctive catalytic performance of **4** is attributed to the redox-active behavior of the metal centers, enhancing the interaction with O_2 molecules. The ORR on a **4**-based catalyst occurs at relatively more positive potentials with lower overpotentials, compared to some previously reported ball-type pentaerythritol-,[10] and dithioerythritol-bridged[24] CoPc-based catalysts. In addition, it was found that the catalytic activity of a **4**-based catalyst towards the ORR in the presence of methanol is better than that of a Pt-based one, suggesting an alternative for DMFC applications.

Acknowledgements

We would like to thank the Commission of Scientific Research Project (BAPKO) of Marmara University [FEN-E-130711-0259] and Turkish Academy of Sciences (TUBA). We also thank Prof. Dr A. Şengül and Dr Z. Odabas for their valuable contribution in drawing some figures.

References

1 A. Y. Tolbin, A. V. Ivanov, L. G. Tomilova and N. S. Zefirov, *J. Porphyrins Phthalocyanines*, 2003, **7**, 162.
2 Y. Tolbin, A. V. Ivanov, L. G. Tomilova and N. S. Zefirov, *Mendeleev Commun.*, 2002, **12**, 96.
3 Z. Odabaş, A. Altındal, A. R. Özkaya, M. Bulut, B. Salih and Ö. Bekaroğlu, *Polyhedron*, 2007, **26**, 695–707.
4 Z. Odabaş, A. Altındal, A. R. Özkaya, M. Bulut, B. Salih and Ö. Bekaroğlu, *Polyhedron*, 2007, **26**, 3505–3512.
5 Z. Odabaş, A. Altındal, M. Bulut, B. Salih and Ö. Bekaroğlu, *Tetrahedron Lett.*, 2007, **48**, 6326–6329.
6 T. Ceyhan, A. Altındal, A. R. Özkaya, Ö. Çelikbıçak, B. Salih, M. K. Erbil and Ö. Bekaroğlu, *Polyhedron*, 2007, **26**, 4239–4249.
7 S. Altun, A. Altındal, A. R. Özkaya, M. Bulut, B. Salih and Ö. Bekaroğlu, *Tetrahedron Lett.*, 2008, **49**, 4483–4486.
8 Ö. Bekaroğlu, *Struct. Bonding*, 2010, **135**, 105 and literature given therein.
9 T. Ceyhan, A. Altındal, A. R. Özkaya, B. Salih and Ö. Bekaroğlu, *Dalton Trans.*, 2009, 10318–10329.
10 İ. Koç, M. Özer, A. R. Özkaya and Ö. Bekaroğlu, *Dalton Trans.*, 2009, 6368–6376.
11 M. Skompska, *Synth. Met.*, 2010, **160**, 1–15.
12 F. B. Kooistra, J. Knol, F. Kastenberg, L. M. Popescu, W. J. H. Verhees, J. M. Kroon and J. C. Hummelen, *Org. Lett.*, 2007, **9**, 551–554.
13 C. J. Brabec, A. Cravino, D. Meissner, N. S. Sariciftci, T. Fromherz, M. T. Rispens, L. Sanchez and J. C. Hummelen, *Adv. Funct. Mater.*, 2005, **11**, 374–380.
14 S. Rajaputra, S. Vallurupalli and V. P. Singh, *J. Mater. Sci.: Mater. Electron.*, 2007, **18**, 1147–1150.
15 S. Senthilarasu, Y. B. Hahn and S. H. Lee, *J. Appl. Phys.*, 2007, **102**, 043512–043516.
16 A. B. P. Lever, E. R. Milaeva and G. Speier, in *Phthalocyanines: Properties and Application*, ed. C. C. Leznoff and A. B. P. Lever, VCH, New York, 1993, vol. 3, pp. 1–69.
17 M. Özer, A. Altındal, A. R. Özkaya, B. Salih, M. Bulut and Ö. Bekaroğlu, *Eur. J. Inorg. Chem.*, 2007, **22**, 3519–3526.
18 W. A. Nevin, W. Liu, S. Greenberg, M. R. Hempstead, S. M. Marcuccio, M. Melnik, C. C. Leznoff and A. B. P. Lever, *Inorg. Chem.*, 1987, **26**, 891–899.
19 M. J. Stillman and A. J. Thomson, *J. Chem. Soc., Faraday Trans. 2*, 1974, **70**, 790–804.
20 C. C. Leznoff, S. M. Marcuccio, S. Greenberg, A. B. P. Lever and K. B. Tomer, *Can. J. Chem.*, 1985, **63**, 623–631.
21 W. A. Nevin, M. R. Hempstead, W. Liu, C. C. Leznoff and A. B. P. Lever, *Inorg. Chem.*, 1987, **26**, 570–577.
22 M. Özer, A. Altındal, A. R. Özkaya and Ö. Bekaroğlu, *Dalton Trans.*, 2009, 3175–3181.
23 Z. Odabaş, A. Altındal, A. R. Özkaya, B. Salih and Ö. Bekaroğlu, *Sens. Actuators, B*, 2010, **145**, 355–366.
24 T. Ceyhan, A. Altındal, A. R. Özkaya, B. Salih and Ö. Bekaroğlu, *Dalton Trans.*, 2010, **39**, 9801–9814.
25 R. C. M. Jakobs, L. J. J. Janssen and E. Barendrecht, *Electrochim. Acta*, 1985, **30**, 1085–1091.
26 S. Marcotte, D. Villers, N. Guillet, L. Rouée and J.-P. Dodelet, *Electrochim. Acta*, 2004, **50**, 179–188.
27 M. Lefevre and J.-P. Dodelet, *Electrochim. Acta*, 2003, **48**, 2749–2760.
28 J. P. Randin, *Electrochim. Acta*, 1974, **19**, 83–85.
29 F. Beck, *J. Appl. Electrochem.*, 1977, **7**, 239–245.
30 J. H. Zagal, *Coord. Chem. Rev.*, 1992, **119**, 89–136.
31 N. Kobayashi and Y. Nishiyama, *J. Phys. Chem.*, 1985, **89**, 1167–1170.
32 N. Kobayashi, P. Janda and A. B. P. Lever, *Inorg. Chem.*, 1992, **31**, 5172–5177.
33 N. Kobayashi and W. A. Nevin, *Appl. Organomet. Chem.*, 1996, **10**, 579–590.
34 L. Zhang, J. Zhang, D. P. Wilkinson and H. Wang, *J. Power Sources*, 2006, **156**, 171–182.
35 S. Baranton, C. Coutanceau, C. Roux, F. Hahn and J.-M. Leger, *J. Electroanal. Chem.*, 2005, **577**, 223–234.
36 Y. Lu and R. G. Reddy, *Electrochim. Acta*, 2007, **52**, 2562–2569.
37 R. Z. Jiang and D. Chu, *J. Electrochem. Soc.*, 2000, **147**, 4605–4609.
38 A. L. Bouwkamp-Wijnoltz, W. Visscher and J. A. R. van Veen, *Electrochim. Acta*, 1998, **43**, 3141–3152.
39 O. Contamin, C. Debiemme-Chouvy, M. Savy and G. Scarbeck, *Electrochim. Acta*, 1999, **45**, 721–729.
40 CAChe WorkSystem Pro Version 6.1.10, 2000–2004, Fujitsu Limited.